



Editor's choice paper

Chemoselective hydrogenation of α,β -unsaturated aldehydes on hydrogenated MoO_x nanorods supported iridium nanoparticles



Sina He^{a,1}, Lifang Xie^{a,1}, Minwei Che^a, Hang Cheong Chan^a, Lichun Yang^{b,*},
Zhangping Shi^c, Yi Tang^c, Qingsheng Gao^{a,*}

^a Department of Chemistry, Jinan University, No. 601 Huangpu Avenue West, 510632 Guangzhou, PR China^b School of Materials Science and Engineering, South China University of Technology, No. 381 Wushan Road, 510640 Guangzhou, PR China^c Department of Chemistry, Shanghai Key Laboratory of Molecular Catalysis and Innovative Materials and Laboratory of Advanced Materials, Fudan University, No. 220 Handan Road, 200433 Shanghai, PR China

ARTICLE INFO

Article history:

Received 2 September 2016

Received in revised form 13 October 2016

Accepted 13 October 2016

Available online 14 October 2016

Keywords:

Hydrogenated molybdenum oxides
Iridium
Metal-support interactions
Chemoselective hydrogenation
 α,β -unsaturated aldehydes

ABSTRACT

As reducible supports, metal oxides present the varied charge effect after hydrogen doping and partial reduction, accomplishing the tunable metal-support interactions and the promoted catalytic turnover in heterogeneous catalysis. Herein, the one-pot fabrication of hydrogenated MoO_x (H-MoO_x) nanorods supported Ir (Ir/H-MoO_x) was developed, which simultaneously combined the generation of active centers (Ir) and the hydrogen doping on supports (H-MoO_x). Because of the accumulated electrons around MoO_6 octahedras after hydrogen doping, the electronic perturbations arising from H-MoO_x supports led to the negatively charged $\text{Ir}^{\delta-}$ species being beneficial for the selective hydrogenation of C=O moiety in α,β -unsaturated aldehydes. In the hydrogenation of cinnamaldehyde to cinnamyl alcohol, Ir/H-MoO_x delivered selectivity as high as ~93%, performing among the best of current metal-based catalysts. Additionally, the efficacy for various substrates with multiple groups further verified our Ir/H-MoO_x system to be competitive for chemoselective hydrogenation.

© 2016 Elsevier B.V. All rights reserved.

1. Introduction

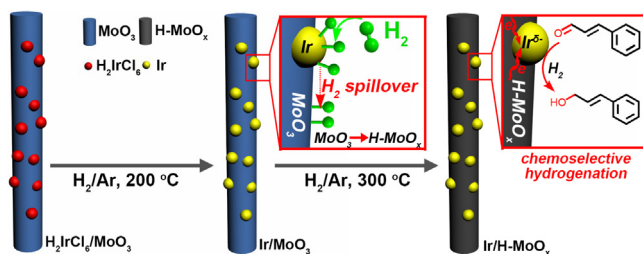
Reducible metal oxides, referring to the metal oxides with variable valence states and relatively easy to be reduced, are promising catalyst supports [1–3]. The partial reduction or hydrogen doping of such oxides results in the emerging “hydrogenated metal oxides” (H-MO_x), which consequently possesses the abundant oxygen vacancies, M-OH and M-H on surface, and more importantly the tuneable band states with metallic features [4–6]. Such variations would further affect the size, morphology, and valence state of loading metals via metal-support interactions, facilitating the achievement of high catalytic conversion with satisfied selectivity [1,3]. Particularly, hydrogenated molybdenum oxides (H-MoO_x) have been highlighted due to the enhanced acidity with H doping and the tailored electronic configuration associated with various valence states (Mo^{6+} , Mo^{5+} , Mo^{4+} , Mo^{3+} and Mo^{2+}) [7,8]. Besides as functional segments in organic optoelectronic devices, photodetectors and energy storage materials [7,9–11], they also

serve as important supports or additives for catalytic hydrogenation [12–16]. On one hand, acidic H-MoO_x is active for the acid-catalyzed ring-opening and cyclization processes, which can provide important synergy towards the selective hydrogenation of biomass-derived oxygenates [15–17]. On the other hand, the abundant oxygen vacancies on H-MoO_x can facilitate the adsorption of oxygen-containing groups (e.g., C=O) in substrates, improving both activity and selectivity in comparison with only metal catalysts [12]. However, the electronic metal-support interactions of H-MoO_x are rarely discussed in this subject, which are reasonably expected in the regard of its metallic band states.

Chemoselective hydrogenation of α,β -unsaturated aldehydes into their corresponding unsaturated alcohols is an important step towards value-added chemicals used in flavorings, perfumes, and pharmaceuticals [18,19]. Due to the higher free reaction enthalpy of C=O (40 kJ mol^{-1}) than that of C=C (35 kJ mol^{-1}), saturated aldehydes instead of desired unsaturated alcohols are the thermodynamically favoured products [19]. It is fundamental and challenging to develop selective catalysts to hydrogenate carbonyl from the conjugated ethylenic (C=C) and carbonyl (C=O) groups. Iridium (Ir) with large d-bands shows high activity for α,β -unsaturated aldehydes hydrogenation, however the selectivity is usually unsatisfied because of the adsorption/activation of both C=C and C=O on the large unoccupied d-orbitals [20,21]. An

* Corresponding authors.

E-mail addresses: mslyang@scut.edu.cn (L. Yang), gaoqingsheng@gmail.com, tqsao@jnu.edu.cn (Q. Gao).¹ These authors contribute equally to this work.



Scheme 1. Schematic illustration for the one-pot fabrication of Ir/H-MoO_x nanorods for chemoselective hydrogenation.

increasing electronic density around Ir is desired to optimize the hydrogenation routes, in which excessive electrons will enhance the repulsive force with C=C, and also promote the electron feedback to π^* in polar C=O [18,22]. Such regulation can be achieved via electronic metal-support interactions on designed supports [4,23]. In the regard of the large-density states around increasing Fermi level (E_F) and the appreciable delocalized electrons [10,24,25], H-MoO_x is expected to present feasible electronic interactions for chemoselective hydrogenation. As evidenced in very recent work, the introduction of H-MoO_x into Ir/SiO₂ catalysts benefited the selective hydrogenation of crotonaldehyde to crotyl alcohol [12], which was ascribed to the promotion of C=O adsorption on H-MoO_x surface, and the electronic metal-support interactions were unfortunately ignored. By contrast, in cinnamaldehyde hydrogenation, the undesired C=C hydrogenation on Pd, rather than C=O, was promoted by using H-MoO_x as the supports [14]. These interesting, but controversial findings indicate the importance of the varied interactions associated with H-MoO_x supports, which needs uncovering and further optimization.

Regarding the feasible hydrogen doping into oxides by H₂ spillover from noble metals [25], we herein develop a one-pot fabrication of H-MoO_x nanorods supported Ir(Ir/H-MoO_x) catalysts for chemoselective hydrogenation. As shown in Scheme 1, Ir nanoparticles (NPs) generate from the reduction of H₂IrCl₆ by H₂/Ar at mild temperature, which serve as active-sites for disassociating H₂ molecules to H atoms upon further heating [26]. The highly active H atoms migrate to the surface of MoO₃, and further diffuse into the bulk, thereby leading to the in-situ hydrogenation of MoO₃. Such fabrication, simultaneously combining the generation of active metal centres and the hydrogen doping on supports, ensures the interactions between ultrafine Ir and fresh H-MoO_x surface. The accumulated electrons around the Mo₆ octahedral of H-MoO_x promote the strong electronic interactions with Ir, resulting in negatively charged Ir^{δ-} species favouring the activation and turnover of C=O. As expected, Ir/H-MoO_x catalysts show high selectivity for the hydrogenation of α,β -unsaturated aldehydes into unsaturated alcohols. In cinnamaldehyde (CAL) hydrogenation, the Ir/H-MoO_x present the cinnamylalcohol (COL) selectivity as high as 93%, outperforming the Ir on other supports (e.g., MoO₃, SiO₂, ZrO₂, and active carbon (AC)) and even conventional metal catalysts. Moreover, the efficacy for various substrates that possess multiple groups (e.g., crotonaldehyde, citral, furfural and nitroarenes) further verifies our Ir/H-MoO_x to be competitive for chemoselective hydrogenation.

2. Experimental

2.1. Catalyst preparation

2.1.1. MoO₃ nanorods

The precursor of Mo₃O₁₀(C₆H₈N)₂·2H₂O nanowires were fabricated according to our previous report [27]. And the MoO₃ nanorods

used as catalyst supports in this work were obtained via calcining Mo₃O₁₀(C₆H₈N)₂·2H₂O at 400 °C for 2 h under air flow.

2.1.2. Ir/H-MoO_x, Ir/MoO₃, Ir/MoO₃(c) (MoO₃(c): commercial MoO₃), Ir/TiO₂, Ir/ZrO₂, Ir/AC, and Ir/SiO₂

Corresponding support was impregnated with H₂IrCl₆ aqueous solution and then stirred at 80 °C for 4 h. The samples were dried at 50 °C overnight, followed by a reduction with a stream of 5 vol% H₂/Ar at 300 °C for 2 h. For Ir/MoO₃, a lower temperature of 200 °C was adopted for the reduction, employing MoO₃ nanorods as the support.

2.1.3. Pt/CNT (CNT: carbon nanotubes) and Ag/SiO₂

CNT or SiO₂ was impregnated with metal-source aqueous solution and then stirred for 4 h at 80 °C. The samples were then dried at 50 °C overnight, followed by a reduction with a stream of 5 vol% H₂/Ar at 300 °C for 2 h.

2.1.4. Au/SiO₂

A typical deposition-precipitation procedure was employed to prepare Au/SiO₂ catalyst. Briefly, SiO₂ was dispersed with the aqueous solution of HAuCl₄, and pH was adjusted to 9.0 by dropwise addition of 0.25 M NH₃·H₂O (aq.). After stirring for 6 h and aging for another 2 h, the catalysts were washed with deionized water for five times and then dried at 50 °C overnight, followed by a reduction with a stream of 5 vol% H₂/Ar at 300 °C for 2 h.

2.2. Physical characterization

X-ray diffraction (XRD) analysis was performed on Bruker D8 diffractometer using Cu K α radiation ($\lambda = 1.54056 \text{ \AA}$). Scanning electron microscopy (SEM) and transmission electron microscopy (TEM) investigations were taken on a ZEISS ULTRA55 and a JEOL JEM 2100F, respectively. Energy dispersive spectrum (EDS) attached on TEM was carried out on a JEOL JEM 2100F. The UV-vis diffuse reflection spectra (UV-vis DRS) were carried out on Varian Cary 5000 at room temperature. X-ray photoelectron spectroscopy (XPS) was processed on a Perkin-Elmer PHI X-tool, using C 1 s (B. E. = 284.6 eV) as a reference. The metal loading was determined by an inductively coupled plasma-atomic emission spectroscopy (ICP-AES). The Brunauer–Emmett–Teller (BET) specific surface areas were determined by adsorption-desorption of nitrogen at liquid nitrogen temperature, using an automatic gas adsorption analyzer (Quantachrome Autosorb-iQ-MP). The hydrogen temperature-programmed reduction (H₂-TPR) and CO chemisorption measurement were both conducted on a XianQuan instrument TP 5076, and the NH₃ temperature-programmed desorption (NH₃-TPD) analysis was carried out on a Micromeritics instrument ChemSorb 2920.

2.3. Catalytic performance measurement

CAL hydrogenation was carried out in a 100 mL stainless steel autoclave (Parr 4848 reactor controller), in which 25 mg of catalyst, 2 mmol of CAL, 20 mL of EtOH and 30 mL of H₂O were loaded. The reactor was sealed and purged with H₂ to remove the air for 3 times, and then the reactor was heated to the desired temperature. Hydrogen (2 MPa) was purged into the reactor after desired temperature was reached and the stirrer was started. The products were analyzed by Shizumadu GC-2014C with a FID detector. The conversion (conv.; %), selectivity to COL and hydrocinnamaldehyde (HCAL) were calculated with the formulas.

$$C_{\text{CAL}} = \frac{N_{\text{CAL},0} - N_{\text{CAL}}}{N_{\text{CAL},0}} \times 100 \quad (1)$$

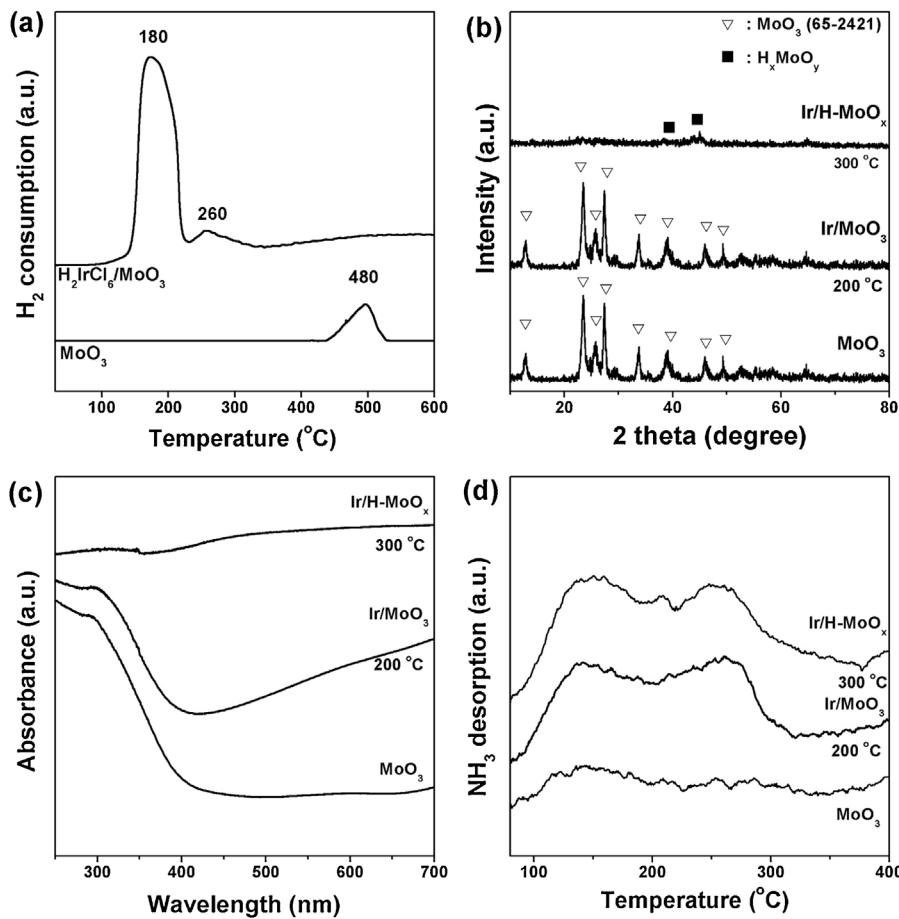


Fig. 1. (a) H₂-TPR profiles of H₂IrCl₆/MoO₃ and bare MoO₃, and (b) XRD, (c) UV-vis DRS and (d) NH₃-TPD profiles of MoO₃ and the corresponding products after Ir loading and H₂ reduction at different temperature.

$$S_i = \frac{N_i}{N_{\text{CAL},0} - N_{\text{CAL}}} \times 100 \quad (2)$$

Where N_{CAL,0} and N_{CAL} are the moles of CAL initially presented in the reactor and the moles of CAL remaining at the time t, respectively; N_i (N_{COL}, N_{H_iCAL}) are the number of moles of COL and HCAL in the mixture at the time t.

3. Results and discussion

One-dimensional (1D) MoO₃ (Fig. S1 in Supplementary materials) derived from Mo₃O₁₀(C₆H₅NH₃)₂·2H₂O nanowires [28] is used the supports in this work (**Scheme 1**). After a typical impregnation with H₂IrCl₆ solution, a reduction by 5 vol.% H₂/Ar is conducted to simultaneously generate Ir NPs and hydrogenate MoO₃ supports at the same time. As indicated by the H₂-TPR results (**Fig. 1a**), the reduction of Ir⁴⁺ to metallic Ir on MoO₃ surface occurs at around 180 °C [29,30]. The following hydrogen consumption at 260 °C should be ascribed to the hydrogenation of MoO₃ surface. By contrast, bare MoO₃ displays a reduction at a higher temperature of 480 °C, which is consistent with previous reports that identified the undetectable reduction by H₂ below 400 °C. The easier reduction is associated with the H₂ spillover from as-form Ir NPs to MoO₃ surface. The chemisorbed hydrogen molecules can dissociate at Ir sites to highly active hydrogen atoms, which migrate to the surface of MoO₃, and further diffuse into the bulk [26,31], thereby accomplishing the in-situ hydrogenation of MoO₃ (**Scheme 1**). As confirmed by XRD analysis (**Fig. 1b**), the product received after a H₂ treatment at 200 °C still remains the phase of orthorhombic MoO₃ (JCPDS No.: 65-2421), the same as the pristine MoO₃.

Such product is thus denoted as Ir/MoO₃. As higher temperature (300 °C) is adopted for reduction, the hydrogenated Ir/H-MoO_x is finally obtained. In its XRD pattern (**Fig. 2b**), the diffraction peaks for MoO₃ disappear, and the new ones at 2θ = 38.1° and 44.1° should be assigned to the as-formed H_xMoO_y [32,33]. Moreover, the above structural evolution is also validated by the UV-vis DRS investigation (**Fig. 1c**). Bare MoO₃ nanorods present a characteristic absorption around 400 nm, consistent with the band gap energy (3.1–3.2 eV) of MoO₃ [25]. A new absorption from 500 to 700 nm emerges in Ir/MoO₃, probably associated with the loading of plasmonic Ir nanostructures and the slight reduction on MoO₃ surface [34]. After the treatment by H₂/Ar at 300 °C, Ir/H-MoO_x displays a wide absorption in UV-vis region, indicating the obvious variation of gap states in MoO₃ due to hydrogen doping and partial reduction [35]. In addition, the acidity of the above samples was determined by means of NH₃-TPD technique (**Fig. 1d**). The amount of NH₃ desorbed from the parent MoO₃ nanorods is negligible, indicating the low density of acidic sites on surface. After the H₂ treatment at 200 and 300 °C, the signal for desorbed NH₃ is greatly improved on Ir/MoO₃ and Ir/H-MoO_x, consistent with the acidic sites arising from H-doping in MoO_x [15]. Regarding the well-retained orthorhombic MoO₃ at 200 °C in XRD, a surface H-doping on Ir/MoO₃ should be suggested, which is not sufficient to alter the crystalline structure inner nanorods. Noticeably, the similar NH₃-TPD signal observed on both Ir/MoO₃ and Ir/H-MoO_x suggests their similarity in surface acidity.

The SEM and TEM investigations were further carried out to characterize the structures of Ir/MoO₃ and Ir/H-MoO_x, with a similar Ir loading of 3.5 ± 0.1 wt%. It is noticed that the metal loading

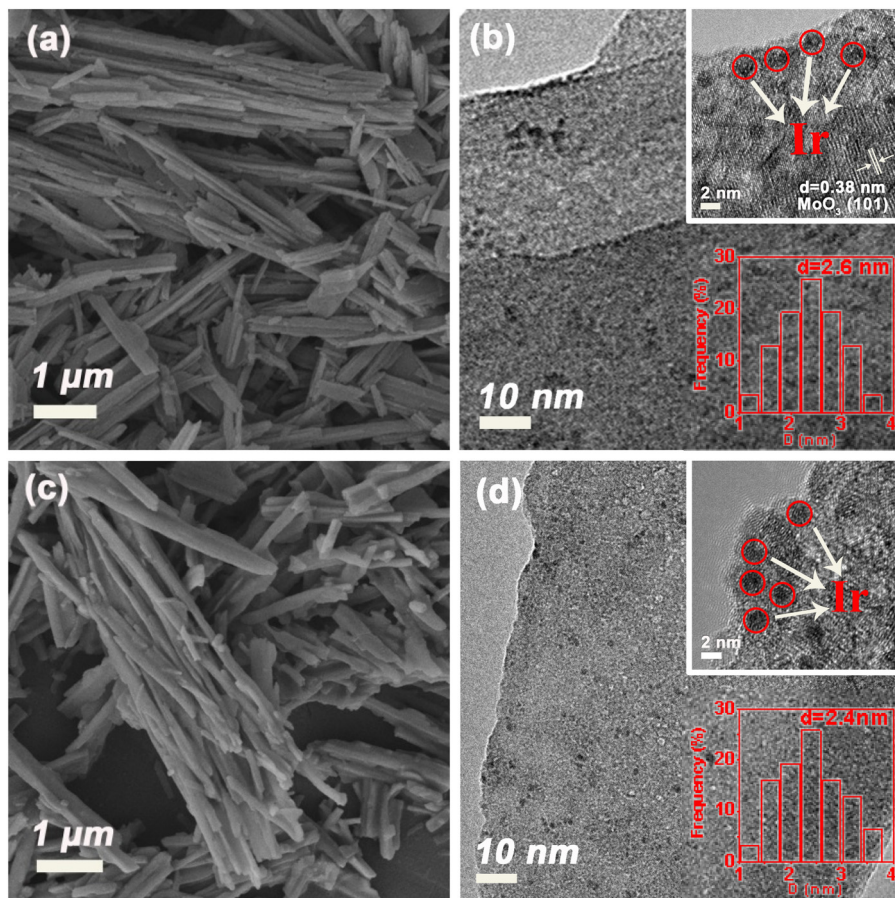


Fig. 2. (a, c) SEM and (b, d) TEM images of (a, b) 3.6%Ir/MoO₃ and (c, d) 3.4%Ir/H-MoO_x. The insets of b and d are the corresponding HR-TEM images and the size-distribution of Ir NPs.

mentioned in this work has been already determined by ICP-AES. As displayed in Fig. 2a and c, the morphology of nanorods inheriting from 1D MoO₃ precursors is observed in SEM for both Ir/MoO₃ and Ir/H-MoO_x. Such 1D nanostructures incline to form interconnecting networks with rich pores, which benefits the dispersion of catalyst in solvent, and more importantly the diffusion of substrates and products during hydrogenation. And, the attached EDS on TEM clearly identify the successful loading of Ir (Fig. S2 in Supplementary materials). The TEM images (Fig. 2b and d) show well-dispersed Ir NPs with a size centered at 2.5 ± 0.1 nm on both MoO₃ and H-MoO_x nanorods. Furthermore, the similarity in Ir size can be validated by the CO uptake analysis of the above samples, which shows the negligible difference (Table S1 in Supplementary materials).

To access the chemical states of above supported Ir relying on supports, XPS analysis focusing on Mo (Fig. 3a) and Ir (Fig. 3b) was conducted. In both Ir/MoO₃ and Ir/H-MoO_x, the Mo 3d profiles can be deconvoluted into four peaks, in which the peaks at 232.5 and 235.6 eV are respectively ascribed to 3d_{5/2} and 3d_{3/2} of Mo⁶⁺, and those at 231.2 and 234.3 eV are associated with Mo⁵⁺ [36]. On the surface of Ir/MoO₃ that is received at 200 °C, dominant Mo⁶⁺ and negligible Mo⁵⁺ species are observed, consistent with the results of H₂-TPR and XRD. With an effective hydrogenation at 300 °C, the Ir/H-MoO_x clearly presents the enriched Mo⁵⁺ in comparison with Mo⁶⁺. This well agrees with the observation in Pd/MoO₃ after a treatment with H₂ flow [25]. Accordingly, obvious electronic metal-support interactions in Ir/H-MoO_x are indicated by the Ir 4f XPS profiles (Fig. 3b). The Ir 4f_{7/2} and 4f_{5/2} at 60.3 and 63.3 eV, respectively, are red-shifted as compared with those of metallic Ir (Ir 4f_{7/2}: 60.8 eV, Ir 4f_{5/2}: 63.8 eV [37]) on MoO₃, and also those on inert SiO₂ support (Fig. S3 in Supplementary materials). This observation well

indicates the negatively charged Ir^{δ-} on H-MoO_x surface. According to the previous experimental discovery and theoretical calculation, the effective hydrogenation of MoO₃ can lead to the metallic band structure with excessive electrons [8,10]. The layered structure of orthorhombic MoO₃ host allows massive H atoms insertion at interlayer positions, which coordinate strongly with terminal oxygen atoms and cause the distortion of MoO₆ octahedras in H-MoO_x framework [25]. Upon adsorption on terminal oxygen atoms, hydrogen atoms become protonic and electron transfers from H 1s orbital to the O 2p orbital [38]. Subsequently, the terminal oxygen atoms transfer charges to the coordinating Mo atoms, thereby causing the partial reduction of molybdenum and the delocalized electrons near E_F in H-MoO_x [25]. Such delocalized electrons donated by penetrating hydrogen will enable the electronic interactions of Ir, resulting in the detectable Ir^{δ-} species. Regarding the repulsive four-electron interactions with C=C and the d-electron feedback into polar C=O both promoted by the enhanced electronic density in Ir [18,22,30], we anticipate that such electronic interactions in Ir/H-MoO_x will benefit the selective hydrogenation of α,β-unsaturated aldehydes.

The benefit of negatively charged Ir^{δ-} on H-MoO_x nanorods in the hydrogenation of α,β-unsaturated aldehydes was demonstrated by the highly selective route for cinnamaldehyde (CAL). As illustrated in Fig. 4, the hydrogenation can proceed either at C=C or C=O group. The former gives saturated aldehyde (hydrocinnamaldehyde, HCAL), and the latter leads to unsaturated alcohol (cinnamyl alcohol, COL), which is industrially desired. As expected, 3.4%Ir/H-MoO_x presents a high selectivity for COL. In the time courses of reaction (Fig. 4), the desired COL is the main product,

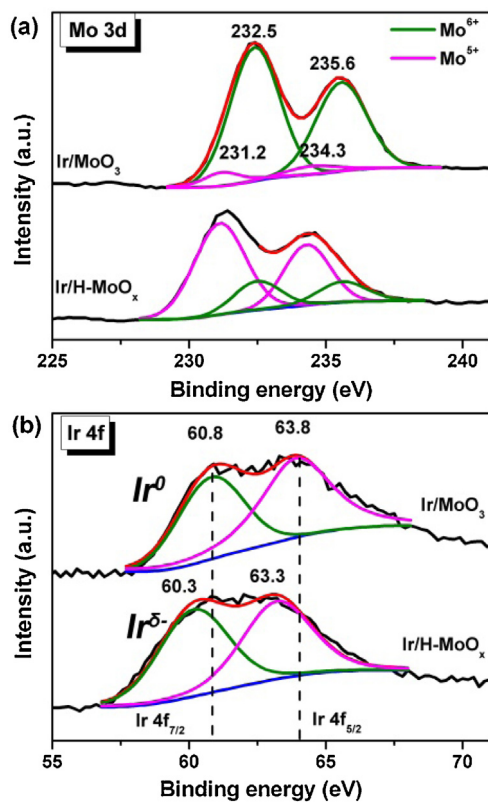
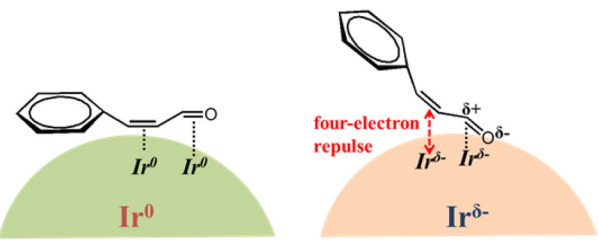


Fig. 3. XPS profiles of (a) Mo 3d and (b) Ir 4f in 3.6%Ir/MoO₃ and 3.4%Ir/H-MoO_x.

and the by-products of HCAL and hydrocinnamal alcohol (HCOL) are limited to a low level. After a reaction for 120 min, an almost complete conversion of CAL is observed, and the distribution of desired COL in the reacting solution is higher than 90%, which well remains even with the prolonged time to 320 min.

The detailed hydrogenation results over supported Ir catalysts are summarized **Table 1**. At the reaction time of 120 min, when the maximum yield of COL is achieved, 3.4%Ir/H-MoO_x shows a COL selectivity as high as 93% with an almost complete CAL conversion (entry 1 in **Table 1**). Regarding the low conversion on bare MoO₃ nanorods at the same condition (entry 2 in **Table 1**), the well-dispersed Ir NPs are believed as the main active species. The COL selectivity of 93% over 3.4%Ir/H-MoO_x is obviously higher than that over 3.6%Ir/MoO₃ (74%, entry 3 in **Table 1**), which can be further confirmed by the initial formation rates of COL ($r_{C=O}$) and HCAL ($r_{C=C}$). Obviously, 3.4%Ir/H-MoO_x presents a much higher $r_{C=O}$ of $803 \mu\text{mol s}^{-1} \text{g}_{\text{Ir}}^{-1}$ than $r_{C=C}$ ($30 \mu\text{mol s}^{-1} \text{g}_{\text{Ir}}^{-1}$).

The TEM (**Fig. 2b** and **d**) and CO uptake (**Table S1** in Supplementary materials) analysis already confirmed the negligible difference in Ir particle size and active-site amounts on H-MoO_x and MoO₃. The surface acidity should be taken into account, because it also affects the adsorption and turnover of CAL [**12,15**]. As attested by the NH₃-TPD result (**Fig. 1d**), the similar signal for desorbed NH₃ on both Ir/MoO₃ and Ir/H-MoO_x can rule out the effect of surface acidity. Thus, it is reasonable to ascribe the improved COL selectivity on Ir/H-MoO_x to the varied electronic configuration associated with the metal-support interactions. It's previously reported that both C=C and C=O can be adsorbed and activated on Ir due to its unoccupied d-orbitals (**Scheme 2**), resulting in the unselective hydrogenation [**20,30,39**]. As the electronic density of Ir increases, the excessive electrons in expanded d-bands would strengthen the four-electron repulsive interactions with non-polar C=C [**18**]. By contrast, the adsorption of polar C^{δ+}=O^{δ-} would be promoted on this negatively charged Ir^{δ-} because of electrostatic interactions,



Scheme 2. Schematic illustration for the varied adsorption of CAL on Ir⁰ and Ir^{δ-} surface, which result from the electronic interactions with different supports, i.e., MoO₃ and H-MoO_x nanorods, respectively. The preferred adsorption of C=O on Ir^{δ-} would lead to the obviously improved selectivity of COL.

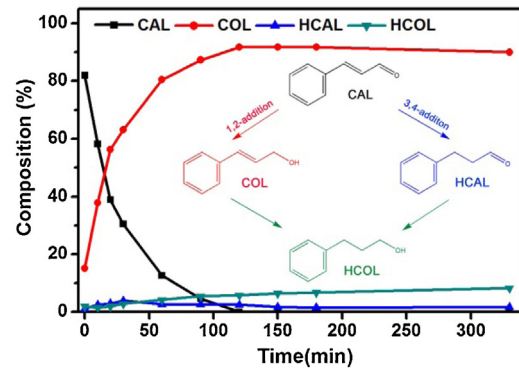


Fig. 4. Time-dependent profile of CAL hydrogenation over 3.4%Ir/H-MoO_x. Inset shows the corresponding reaction pathways.

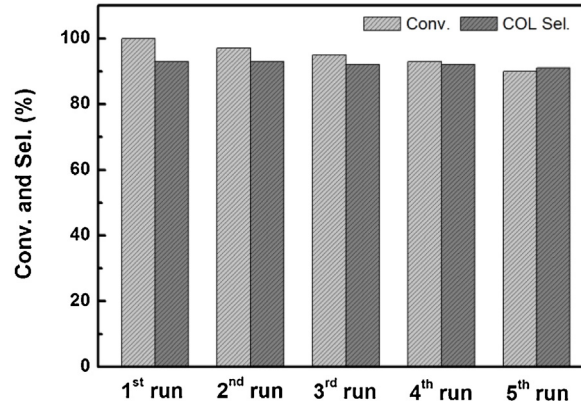


Fig. 5. CAL hydrogenation over 3.4%Ir/H-MoO_x for five successive runs, showing the CAL conversion and COL selectivity at the time of 120 min.

and even its activation due to the electron feedback to π* of C=O [**18,22,40**]. As a result, such negatively charged Ir^{δ-} on H-MoO_x, distinguished from the metallic Ir⁰ on inert MoO₃, contributes to the highly selective hydrogenation of C=O. Although H_xMoO₃ has been ever introduced as supports for Pd in CAL hydrogenation, the C=C hydrogenation was unfortunately preferred [**14**]. In the control experiment of this work, the 3.4%Pd/H-MoO_x shows the unselective hydrogenation for CAL ($t = 60$ min, $C_{\text{CAL}} > 99\%$, $S_{\text{COL}} < 25\%$). It's believed that the nature of various metals make obvious influence on their interactions with H-MoO_x, which is of great importance for the chemoselective hydrogenation.

The selective hydrogenation on Ir/H-MoO_x is affected by the nature of the H-MoO_x and Ir loading, as a result of their interactions. As commercial MoO₃ with micron size is employed as supports (denoted as Ir/MoO₃(c)), the CAL conversion (32%) is lower than that on Ir/H-MoO_x, although the COL selectivity remains >90% (entry 4 in **Table 1**). The reduced activity can be ascribed to the

Table 1Hydrogenation results of CAL over supported Ir catalysts and other counterparts^a.

Entry	Catalysts	Time (min)	Conv. (%)	Sel. (%)		Initial rate ^c	
				COL	HCAL	$r_{C=O}$	$r_{C=C}$
1	3.4%Ir/H-MoO _x	120 ^b	>99	93	2	807	30
2	MoO ₃	120	5	82	15	/	/
3	3.6%Ir/MoO ₃	120	78	76	8	280	13
4	3.5%Ir/MoO ₃ (c)	120	32	91	5	118	3
5	2.8%Ir/H-MoO _x	120 ^b	92	91	3	691	44
6	5.6%Ir/H-MoO _x	120 ^b	>99	90	2	656	43
7	8.5%Ir/H-MoO _x	120 ^b	>99	85	2	365	10
8	3.8%Ir/TiO ₂	270 ^b	98	64	7	187	13
9	3.6%Ir/ZrO ₂	270 ^b	89	77	10	226	26
10	3.2%Ir/AC	390 ^b	41	68	25	31	21
11	3.5%Ir/SiO ₂	270 ^b	81	78	12	177	15
12	3.9%Pt/CNT	120 ^b	87	52	46	296	64
13	3.8%Au/SiO ₂	270 ^b	69	70	21	75	13
14	3.2%Ag/SiO ₂	270 ^b	79	72	18	85	21

^a Reaction condition: catalyst (25 mg), CAL (2 mmol), H₂O (30 mL), EtOH (20 mL), temperature (100 °C), H₂ (2 MPa), stirring rate (600 rpm).^b Values corresponding to the maximum yield of CROL.^c Value calculated from the time-profiles in the beginning of reaction, in term of $\mu\text{mol s}^{-1} \text{g}_{\text{metal}}^{-1}$.**Table 2**Chemoselective hydrogenation of various substrates that possess multiple reducible groups over Ir/H-MoO_x^a.

Substrate	Product	solvent	T (°C)	t (h)	Conv. (%)	Sel. (%)		
	crotonaldehyde (2.0 mmol)		crotyl alcohol	H ₂ O (50 mL)	100	3.0	88	66
	E/Z-citral (2.0 mmol)		geraniol + nerol	H ₂ O (30 mL)/EtOH (20 mL)	100	3.0	95	96
	furfural (6 mmol)		furfuryl alcohol	H ₂ O (10 mL)	30	6.0	98	99
	4-chloronitrobenzene (1.0 mmol)		4-chloroaniline	EtOH (30 mL)	40	2.0	61	90
	1-bromo-4-nitrobenzene (1.0 mmol)		4-bromoanilines	EtOH (30 mL)	40	2.0	66	96
	4-nitrobenzoic acid (1.0 mmol)		4-aminobenzoic acid	EtOH (30 mL)	60	2.0	94	99

^a Reaction condition: catalyst (25 mg), H₂ (2 MPa), stirring rate (600 rpm).

small surface of bulky MoO₃ ($S_{\text{BET}} < 5 \text{ m}^2 \text{ g}^{-1}$, Table S1 and Fig. S4 in Supplementary materials), while, the electronic metal-support interactions arising from hydrogenated supports is still available for selective hydrogenation. Meanwhile, the evolving catalytic performance associated with Ir loading from 2.8% to 8.5% (entries 6–8 in Table 1) suggests the optimized loading around 3.4%. With a low Ir loading (2.8–5.6%), the selectivity of C=O remains at a level higher than 90%, which should be ascribed to the small Ir ($2.4 \pm 0.1 \text{ nm}$, Fig. S5 in Supplementary informations) with sufficient metal-support interactions. By contrast, the selectivity slightly decreases at a high Ir loading (e.g., 8.5%Ir/H-MoO_x), probably due to the prohibited interactions at enlarged Ir nanoparticles (3.0 nm).

Our 3.4%Ir/H-MoO_x is featured by its both high selectivity and activity, in comparison with Ir on other supports (entries 8–11 in Table 1), e.g., TiO₂, ZrO₂, AC, and SiO₂. This highlights the importance of interactions between H-MoO_x and Ir for selectively hydrogenating CAL with a good efficiency. The performance of 3.4%Ir/H-MoO_x also outperforms those of conventional met-

als (entries 12–14 in Table 1), e.g., Pt/CNT, Au/SiO₂ and Ag/SiO₂. The selectivity of 93% over Ir/H-MoO_x is also superior to those of recently reported Ir (Ir/CNT, 68%, Au-Ir/TiO₂, 83%), Pt-on-Au nanostructures (<80%) and metal-organic-framework-confined Pt (91%) [41–43], and comparable to ligand-capped PtFe (94%) [44].

Additionally, a recycle test for the Ir/H-MoO_x is carried out to investigate its service life. As shown in Fig. 5, the catalyst delivers the high catalytic performance even after five successive cycles. The similar COL selectivity at a high level >90% indicates the well-retained catalytic nature of Ir/MoO_x. The slight decrement of activity during cycling is probably due to the inevitable loss of catalysts in recovery by centrifugation, because no Ir is detected in residual reaction solution by ICP-AES analysis.

More importantly, our Ir/H-MoO_x can be considered in a sense as a universal catalyst for chemoselective hydrogenation, especially for the substrates with various reducible groups (Table 2). In the case of α,β -unsaturated aldehydes, 3.4%Ir/H-MoO_x presents the high selectivity of unsaturated alcohols in crotonaldehyde (~66%),

citral (~96%) and furfural (99%). The steric effects on selective α,β -unsaturated aldehydes hydrogenation have been previously demonstrated, the more steric prohibition of C=C by the substitutes at γ -carbon, the higher C=O selectivity [18,45]. In the case of crotonaldehyde, the relatively lower selectivity, as compared with those in CAL, citral and furfural, is associated with the negligible steric hindrance effects of a small methyl at γ -carbon. Meanwhile, as for substituted nitroarenes, in which the target nitro with polarity prefers the adsorption on Ir $^{\delta-}$ sites [46], Ir/H-MoO_x also displays the highly selective routes towards the corresponding functionalized anilines. The selectivity of aromatic anilines is 90%, 96% and 99% for 4-chloronitrobenzene, 1-bromo-4-nitrobenzene and 4-nitrobenzoic acid, respectively. These results well verify Ir/H-MoO_x as a promising catalyst for chemoselective hydrogenation.

4. Conclusions

In summary, H₂ spillover on in-situ formed Ir NPs was utilized to hydrogenate MoO₃ supports on-site, accomplishing the highly selective catalyst of Ir/H-MoO_x nanorods for chemoselective hydrogenation. The active Ir $^{\delta-}$ species on H-MoO_x due to the strong electronic metal-support interactions is responsible for the selective C=O hydrogenation. Such innovation also promotes the selective hydrogenation of a wide range of organics with multiple groups, verifying the importance of support interactions associated with hydrogenated metal oxides. It is envisioned that the future work with more precise control over hydrogenated supports would further boost the relevant catalytic applications.

Acknowledgements

This work is financially supported by National Basic Research Program of China (2013CB934101), National Natural Science Foundation of China (21373102, 21433002, 51671089 and 51402110), Guangdong Natural Science Funds for Distinguished Young Scholar (2015A030306014), Guangdong Program for Support of Top-notch Young Professionals (2014TQ01N036), Guangdong Higher Education Institute (YQ2013022), and Fundamental Research Funds for the Central Universities (21615402).

Appendix A. Supplementary data

Supplementary data associated with this article can be found, in the online version, at <http://dx.doi.org/10.1016/j.molcata.2016.10.016>.

References

- [1] Q. Fu, T. Wagner, *Surf. Sci. Rep.* 62 (2007) 431–498.
- [2] G.A. Somorjai, J.Y. Park, *Angew. Chem. Int. Ed.* 47 (2008) 9212–9228.
- [3] X.Y. Liu, A. Wang, T. Zhang, C.-Y. Mou, *Nano Today* 8 (2013) 403–416.
- [4] J.Y. Park, L.R. Baker, G.A. Somorjai, *Chem. Rev.* 115 (2015) 2781–2817.
- [5] X. Chen, L. Liu, F. Huang, *Chem. Soc. Rev.* 44 (2015) 1861–1885.
- [6] X. Sun, Y. Guo, C. Wu, Y. Xie, *Adv. Mater.* 27 (2015) 3850–3867.
- [7] D. Xiang, C. Han, J. Zhang, W. Chen, *Sci. Rep.* 4 (2014) 4891.
- [8] W. Xie, M. Su, Z. Zheng, Y. Wang, L. Gong, F. Xie, W. Zhang, Z. Luo, J. Luo, P. Liu, N. Xu, S. Deng, H. Chen, J. Chen, *ACS Nano* 10 (2016) 1662–1670.
- [9] M.M.Y.A. Alsait, K. Latham, M.R. Field, D.D. Yao, N.V. Medehkar, G.A. Beane, R.B. Kaner, S.P. Russo, J.Z. Ou, K. Kalantar-zadeh, *Adv. Mater.* 26 (2014) 3931–3937.
- [10] P.-R. Huang, Y. He, C. Cao, Z.-H. Lu, *Sci. Rep.* 4 (2014) 7131.
- [11] X. Xiao, Z. Peng, C. Chen, C. Zhang, M. Beidaghi, Z. Yang, N. Wu, Y. Huang, L. Miao, Y. Gogotsi, J. Zhou, *Nano Energy* 9 (2014) 355–363.
- [12] M. Tamura, K. Tokonami, Y. Nakagawa, K. Tomishige, *ACS Catal.* 6 (2016) 3600–3609.
- [13] T. Matsuda, F. Uchijima, H. Sakagami, N. Takahashi, *Phys. Chem. Chem. Phys.* 3 (2001) 4430–4436.
- [14] M. Kołodziej, A. Drelinkiewicz, E. Lalik, J. Gurgul, D. Duraczyńska, R. Kosydar, *Appl. Catal. A: Gen.* 515 (2016) 60–71.
- [15] J. Guan, G. Peng, Q. Cao, X. Mu, *J. Phys. Chem. C* 118 (2014) 25555–25566.
- [16] K.-i. Shimizu, S. Kanno, K. Kon, *Green Chem.* 16 (2014) 3899.
- [17] S. Koso, N. Ueda, Y. Shinmi, K. Okumura, T. Kizuka, K. Tomishige, *J. Catal.* 267 (2009) 89–92.
- [18] P. Gallezot, D. Richard, *Catal. Rev. Sci. Eng.* 40 (1998) 81–126.
- [19] P. Mäki-Arvela, J. Hájek, T. Salmi, D.Y. Murzin, *Appl. Catal. A* 292 (2005) 1–49.
- [20] B.F. Machado, H.T. Gomes, P. Serp, P. Kalck, J.L. Faria, *ChemCatChem* 2 (2010) 190–197.
- [21] P. Reyes, M.C. Aguirre, I. Melian-Cabrera, M.L. Granados, J.L.G. Fierro, *J. Catal.* 208 (2002) 229–237.
- [22] C.Y. Hsu, T.C. Chiu, M.H. Shih, W.J. Tsai, W.Y. Cheu, C.H. Liu, *J. Phys. Chem. C* 114 (2010) 4502–4510.
- [23] Y. Bai, W.H. Zhang, Z.H. Zhang, J. Zhou, X.J. Wang, C.M. Wang, W.X. Huang, J. Jiang, Y.J. Xiong, *J. Am. Chem. Soc.* 136 (2014) 14650–14653.
- [24] M. Vasiliopoulos, A.M. Douvas, D.G. Georgiadou, L.C. Palilis, S. Kennou, L. Sygellou, A. Soulati, I. Kostis, G. Papadimitriopoulos, D. Davazoglou, P. Argitis, *J. Am. Chem. Soc.* 134 (2012) 16178–16187.
- [25] H.F. Cheng, M.C. Wen, X.C. Ma, Y. Kuwahara, K. Mori, Y. Dai, B.B. Huang, H. Yamashita, *J. Am. Chem. Soc.* 138 (2016) 9316–9324.
- [26] R. Prins, *Chem. Rev.* 112 (2012) 2714–2738.
- [27] Q. Gao, S. Wang, H. Fang, J. Weng, Y. Zhang, J. Mao, Y. Tang, *J. Mater. Chem.* 22 (2012) 4709–4715.
- [28] L.C. Yang, S.N. Wang, J.J. Mao, J.W. Deng, Q.S. Gao, Y. Tang, O.G. Schmidt, *Adv. Mater.* 25 (2013) 1180–1184.
- [29] W. Lin, H. Cheng, L. He, Y. Yu, F. Zhao, *J. Catal.* 303 (2013) 110–116.
- [30] S.N. He, Z.J. Shao, Y.J. Shu, Z.P. Shi, X.M. Cao, Q.S. Gao, P.J. Hu, Y. Tang, *Chem. Eur. J.* 22 (2016) 5698–5704.
- [31] M. Choi, S. Yook, H. Kim, *ChemCatChem* 7 (2015) 1048–1057.
- [32] H. Sakagami, T. Ohno, H. Itoh, Z. Li, N. Takahashi, T. Matsuda, *Appl. Catal. A: Gen.* 470 (2014) 8–14.
- [33] T. Matsuda, H. Sakagami, N. Takahashi, *Catal. Today* 81 (2003) 31–42.
- [34] K. Chakrapani, S. Sampath, *Chem. Commun.* 50 (2014) 3061–3063.
- [35] S. Balendran, J. Deng, J.Z. Ou, S. Walia, J. Scott, J. Tang, K.L. Wang, M.R. Field, S. Russo, S. Zhuiykov, M.S. Strano, N. Medhekar, S. Sriram, M. Bhaskaran, K. Kalantar-zadeh, *Adv. Mater.* 25 (2013) 109–114.
- [36] J. Baltrusaitis, B. Mendoza-Sanchez, V. Fernandez, R. Veenstra, N. Dukstiene, A. Roberts, N. Fairley, *Appl. Surf. Sci.* 326 (2015) 151–161.
- [37] F. Heroguel, G. Siddiqi, M.D. Detwiler, D.Y. Zemlyanov, O.V. Safonova, C. Copret, *J. Catal.* 321 (2015) 81–89.
- [38] X.W. Sha, L. Chen, A.C. Cooper, G.P. Pez, H.S. Cheng, *J. Phys. Chem. C* 113 (2009) 11399–11407.
- [39] P. Reyes, H. Rojas, G. Pecchi, J.L.G. Fierro, *J. Mol. Catal. A: Chem.* 179 (2002) 293–299.
- [40] M. Bidaoui, C. Espeel, S. Sabour, L. Benatallah, N. Saib-Bouchenafa, S. Royer, O. Mohammedi, *J. Mol. Catal. A* 399 (2015) 97–105.
- [41] J. Zhao, J. Ni, J. Xu, J. Xu, J. Cen, X. Li, *Catal. Commun.* 54 (2014) 72–76.
- [42] K.-Q. Sun, Y.-C. Hong, G.-R. Zhang, B.-Q. Xu, *ACS Catal.* 1 (2011) 1336–1346.
- [43] Z.Y. Guo, C.X. Xiao, R.V. Maligal-Ganesh, L. Zhou, T.W. Goh, X.L. Li, D. Tesfagaber, A. Thiel, W.Y. Huang, *ACS Catal.* 4 (2014) 1340–1348.
- [44] K.B. Vu, K.V. Bukhryakov, D.H. Anjum, V.O. Rodinov, *ACS Catal.* 5 (2015) 2529–2533.
- [45] T.B.L.W. Maeinelli, S. Nabuurs, V. Ponec, *J. Catal.* 151 (1995) 431–438.
- [46] X.Y. Yang, S.N. He, Y.J. Shu, Z.P. Shi, Y.L. Guo, Q.S. Gao, Y. Tang, *RSC Adv.* 5 (2015) 89282–89289.